Research Article | Vol. 27, No. 4 | 18 Feb 2019 | OPTICS EXPRESS 5598
Optics EXPRESS

ICL-based mid-infrared carbon dioxide sensor system for deep-sea natural gas hydrate exploration

Zhiwei Liu,[1] Chuantao Zheng,[1,4,5] Chen Chen,[2,6] Yafei Li,[1] Hongtao Xie,[1] Qiang Ren,[2] Yiding Wang,[1] AND Frank K. Tittel[3]

[1]*State Key Laboratory of Integrated Optoelectronics, College of Electronic Science and Engineering, Jilin University, 2699 Qianjin Street, Changchun 130012, China*
[2]*College of Instrumentation & Electrical Engineering, Jilin University, 938 Ximinzhu Street, Changchun 130021, China*
[3]*Department of Electrical and Computer Engineering, Rice University, 6100 Main Street, Houston, TX 77005, USA*
[4]*Correspondence should be addressed here*
[5]*zhengchuantao@jlu.edu.cn*
[6]*cchen@jlu.edu.cn*

Abstract: For deep-sea natural gas hydrate exploration, highly sensitive detection of the dissolved gas in seawater near the seabed is significant because it requires the sensor system to be small in size, low in power consumption, and high in sensitivity. A mid-infrared sensor system was developed to detect dissolved carbon dioxide (CO_2) in sea-water, while employing a 4319 nm continuous-wave interband cascade laser (ICL) and a multi-pass gas cell (MPGC) with a 29.8 m optical path length. A compact rectilinear optical structure was proposed by using the free-space-emitting ICL and tunable laser absorption spectroscopy (TLAS). This leads to a minimized sensor size and a simple optical alignment for deep-sea operation. A strong CO_2 absorption line, located at 2315.19 cm^{-1} and a weak 2315.28 cm^{-1} line and at a low pressure of 40 Torr, was targeted for low- and high-concentration CO_2 detection within a concentration range of 0-1000 parts per billion by volume (ppbv) and 0-40 parts per million by volume (ppmv), respectively. The limit of detection (LoD) was assessed to be 0.72 ppbv at an averaging time of 2 s, and the response time was measured to be ~30 s at a flow rate of ~180 standard cubic centimeters per minute (sccm). Deployment of the CO_2 sensor combined with a gas-liquid separator was carried out for the CO_2 detection in the gas extracted from water, which validated the reported sensor system's potential application for deep-sea natural gas hydrate exploration.

1. Introduction

Natural gas hydrate, regarded as a potential alternative for rapidly consumed fossil fuels nowadays, is a new type of energy material deposited diffusely on the worldwide seabed [1,2]. Great effort has been made for the exploration and trial mining of this kind of energy. One significant research is to make a detailed composition analysis of the natural gas hydrate, for determining its origin and speeding up the pace of utilization. To investigate the composition of natural gas hydrate accurately, *in situ* detection of gas species dissolved in seawater near the sediments is an efficient way. The gas species to be detected mainly include methane (CH_4) and carbon dioxide (CO_2), which are generated from the slow decomposition of gas hydrate under a specific condition [3–5]. For this purpose, because of good *in situ* performance and high precision up to a concentration level of parts per billion in volume (ppbv), geochemical analytical methods (e.g. mass spectrometry and Raman spectrum analysis) [6] have been increasingly employed rather than geophysical methods (e.g. marine deep-tow seismic technique) [7]. However, these techniques usually need large-size and

#357434 https://doi.org/10.1364/OE.27.005598
Journal © 2019 Received 11 Jan 2019; accepted 8 Feb 2019; published 13 Feb 2019

Optics EXPRESS

complicated facilities with relatively high power consumption, increasing the difficulty in the realization of gas detection in deep-sea. Moreover, a long-time pre-treatment of gas sample is usually required so that the response time is significantly increased to up to several minutes.

Infrared laser absorption spectroscopy [8–12] based gas sensing techniques have great potential for gas detection in deep-sea environment in terms of sensor size, cost, power consumption and response time. One typical and developed technique is tunable laser absorption spectroscopy (TLAS) [13–15], which is regarded as an excellent tool for trace gas detection in many fields, such as environmental monitoring [16–18] and industrial application [19,20]. Since the invention of interband cascade laser (ICL) in 1999 [21–23], this kind of mid-infrared light source has been widely used in gas detection because of its low power consumption and the strong absorption of many gas species in the mid-infrared waveband [24–26]. However, because of the free-space emitting characteristics of this type of mid-infrared laser, an optical alignment structure should be designed for tracing the invisible infrared beam [27]. Moreover, a signal processing system with simple structure and small space occupation is also needed to automatically harmonize the sensor system operation and communicate with the upper workstation on the tow-ship.

Combining with a gas-liquid separator, a TLAS based sensor is able to provide an *in situ* measurement of gas extracted from seawater with a precision up to ppbv-level with a special design. For this purpose, aiming at size minimization, structure simplification, cost saving and operation automatization, a mid-infrared CO_2 sensor system, for the first time to the best of our knowledge, was developed for natural gas hydrate exploration in deep-sea. The two CO_2 absorption lines at 2315.19 cm^{-1} and 2315.28 cm^{-1} in the mid-infrared waveband were chosen as the target to realize a wide range detection at low pressure, and a 4319 nm ICL with a driving current of only ~50 mA was employed as the optical source. A compact rectilinear optical structure was designed for coupling the ICL beam to a multi-pass gas cell (MPGC) and a mid-infrared detector, which simplified the optical part of the sensor. The electrical part was custom-made for low power consumption, miniaturized integration and long-distance communication with the upper computer. The sensor system was integrated into a standalone barrel-shape system for the operation in the high-pressure underwater environment. A series of experiments were carried out in laboratory to evaluate the performance of the sensor for CO_2 detection. Also, together with a gas-liquid separator system, a gas detection experiment was performed to verify the normal operation of the sensor system for the detection of the extracted gas from water.

2. Sensor design and optimization

2.1 Compact rectilinear optical structure

A compact optical structure was designed for coupling the mid-infrared free-space-emitting laser beam into the gas cell and delivering the output to the detector, as exhibited in Fig. 1(a). An ICL (Nanoplus, Germany) emitting at 4319 nm was employed to generate infrared light within a specific wavelength range for targeting the selected CO_2 absorption line. A MPGC with a physical size of 20 × 16 × 5 cm^3 provides a sealed environment for the interaction between the infrared light and the target gas and offers a 29.8 m effective optical path length after 215 reflections. A mercury-cadmium-telluride (MCT) detector (VIGO System, Model PVI-4TE-5) was used to convert the absorbed infrared light to an electrical signal. For sensor size minimization, the three optical modules were arranged along a straight line, resulting in a small cubic volume of 48 × 19 × 13.5 cm^3 for the whole optical system including the baseplate. This is nearly the minimum volume that can be achieved with the absence of all beam-guiding optical elements.

Optics EXPRESS

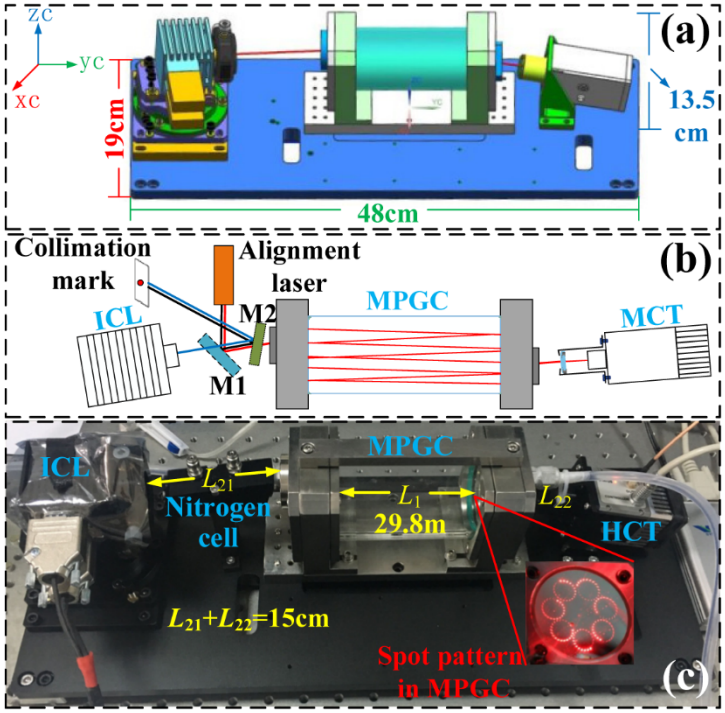

Fig. 1. (a) CAD image of the proposed rectilinear optical structure with a cubic volume of 48 × 19 × 13.5 cm^3. (b) Schematic of the alignment procedure of the compact optical structure. (c) Photograph of the established rectilinear optical structure with a reference cell filled with N_2 placed between the ICL and the MPGC. The spot pattern in the MPGC is shown by the insert in Fig. 1(c). ICL: interband cascade laser; M1, M2: plane mirror; MPGC: multi-pass gas cell; MCT: mercury-cadmium-telluride detector.

A 635 nm visible laser and two plane mirrors were used for beam tracing, which is described in Fig. 1(b). There are three alignment steps, in which the beam paths are represented by lines in red (step 1), black (step 2) and blue (step 3), respectively. Step 1: Guide the red alignment beam into the MPGC with the help of a plane mirror (M1) and obtained a specific spot pattern shown by the insert in Fig. 1(c), which means that the optimum incident angle was found. M1 was installed on a 90°flip mount (Thorlabs, Model FM90/M), which could be overturned up and down repetitively to switch the light source between the ICL and the alignment laser. Step 2: Another plane mirror (M2) was placed in front of the MPGC to reflect the visible beam to the direction towards a collimation mark, which was a paper board used to record the path of the reflection beam. Step 3: The ICL was turned on and M1 was switched off to make the infrared light be reflected to the collimation mark. A multi-dimensional adjustable mount for ICL was fabricated to slightly change the position and emitting angle of the laser beam. With a thermal-sensitive laser viewing card, the path of the infrared light was observed and adjusted to coincide with the recorded path of the alignment beam. Finally, the invisible infrared light was successfully traced by the visible beam from the alignment laser.

After removing the alignment elements, the rectilinear optical structure was formed as shown in Fig. 1(c). The optical path length can be divided into two sections, including L_1 (inside the gas cell, 29.8 m) and L_2 (outside the gas cell, L_{21} + L_{22} = 15 cm), resulting in an absorbed infrared light intensity expressed based on the Beer-Lambert law as

$$I(\upsilon) = I_0 \bullet \exp[-\alpha_1(\upsilon)C_1L_1] \bullet \exp[-\alpha_2(\upsilon)C_2L_2] \quad (1)$$

Optics EXPRESS

where I_0 is the initial light intensity of the ICL, $\alpha_1(v)$ and $\alpha_2(v)$ are the absorption coefficients of CO_2 molecule at the pressure inside and outside the gas cell, respectively, C_1 and C_2 are the CO_2 concentrations inside and outside the gas cell, respectively. Because of the high concentration of CO_2 in the air, the absorption outside the gas cell makes considerable contribution to the detection, which is named background absorption. To decrease the background absorption as much as possible, a small gas cell full of nitrogen (N_2) with an optical path of 7 cm was fabricated and fixed between the ICL and the MPGC for reducing the background influence by decreasing the path length of L_2.

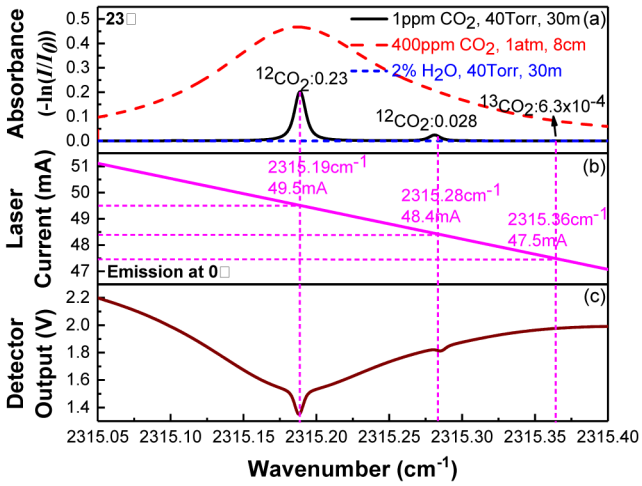

Fig. 2. (a) HITRAN based absorption spectra of CO_2 (1 ppmv) and H_2O (2%) at a pressure of 40 Torr and an optical length of 30 m and CO_2 (400 ppmv) at a pressure of 1 atm and an optical length of 8 cm, which are shown in black, blue and red, respectively, at 23 °C. (b) Plot of the ICL emission wavenumber as a function of the ICL drive current at a laser operation temperature of 0 °C. (c) Output signal from the detector indicating a comprehensive absorption at high pressure (background) and low pressure (target).

2.2 Selection of CO_2 absorption line

To enhance the detection precision of the sensor, the used CO_2 absorption line was selected from the mid-infrared waveband, where the line strength can be up to four orders of magnitude higher than those in the near-infrared waveband. As shown by the red dash line in Fig. 2(a), at a 1 atm pressure, a strong absorption line for a high-precision detection of CO_2 is located at 2315.19 cm^{-1}, whose strength is 1.963×10^{-19} cm/molecule at a temperature of 23°C and a pressure of 1 atm. Considering that the extracted gas from sea water is quite limited, the expected gas pressure in the gas cell cannot be high (e.g. < 100 Torr). Therefore, with a low pressure of 40 Torr and an optical path of ~30 m, Fig. 2(a) depicts some narrow absorption lines based on the high resolution transmission (HITRAN) database for a 1 parts per million by volume (ppmv) CO_2, which includes a strong $^{12}CO_2$ absorption line at 2315.19 cm^{-1}, a weak $^{12}CO_2$ absorption line at 2315.28cm^{-1} and a $^{13}CO_2$ absorption line at 2315.36 cm^{-1}. The absorption of H_2O with a concentration level of 2% shows no influence to CO_2 detection. According to the linear relation between the ICL emitting wavenumber and driving current plotted in Fig. 2(b), the current range was decided to be 47–51 mA to simultaneously scan the three CO_2 lines.

For the proposed optical structure, an additional absorption with a gas pressure of 1 atm and an optical path length of 8 cm should also be considered, which can be treated as background absorption. A simulation of CO_2 background absorption was performed, where the CO_2 concentration is assumed to be 400 ppmv (i.e. normal atmospheric CO_2 concentration), as shown by the red dash line in Fig. 2(a). The absorbance is higher than those

Optics EXPRESS

at 40 Torr pressure and 30 m path length, and the line with a large width covering the three narrow lines. Due to a superposition of the background absorption and the target absorption, an example of the generated signal from the detector is shown in Fig. 2(c). The influence of the background absorption can be removed by using lock-in detection due to a large line width difference between 1 atm and 40 Torr, and the CO_2 concentration can be derived by analyzing the narrow absorption peaks after removing the smooth background signal.

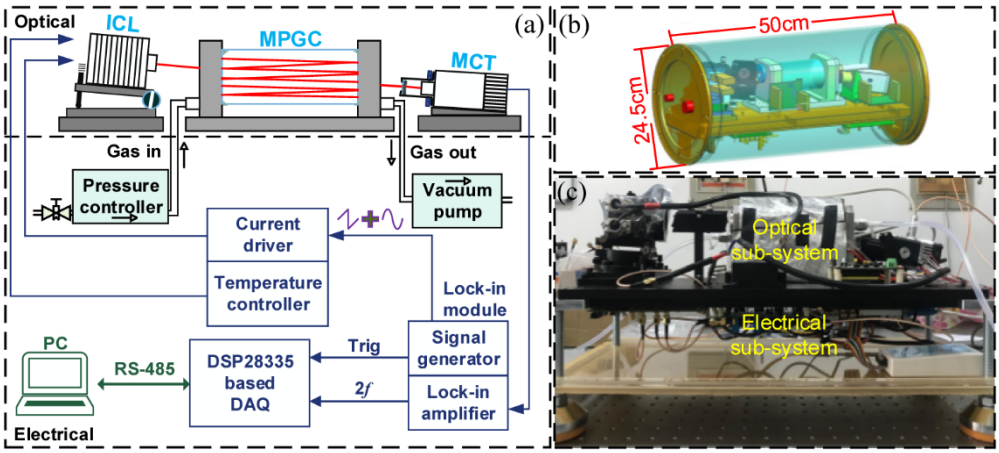

Fig. 3. (a) Schematic diagram of the mid-infrared CO_2 sensor system including an electrical sub-system and an optical sub-system. (b) CAD image of the barrel-shape equipment for the sensor integration with a diameter of 24.5 cm and a length of 50 cm. (c) Photograph of the integrated sensor system without the shield.

2.3 Sensor system design

Employing the rectilinear optical structure, a wavelength modulation spectroscopy (WMS) [28,29] based CO_2 sensor system was designed. Figure 3(a) describes the structure of the optical sub-system and electrical sub-system. In the electrical part, a compact laser driver (Wavelength Electronics, Model LDTC0520) integrated with a temperature controller and a current driver was used for stabilizing the laser temperature and providing current for the laser. A field-programmable gate array (FPGA) based lock-in module with two independent channels was used for signal processing, including generating a saw-tooth scan signal superimposed by a sinusoid modulation signal for the current driver and extracting the 2*f* signal from the MCT detector's output. A digital signal processor (DSP, Texas Instruments, Model TMS320F28335) based data acquisition (DAQ) module was used for 2*f* signal acquisition triggered by the second channel of the lock-in module. The DSP also delivered 2*f*-amplitude, concentration and the sensor's operation state parameters to a laptop for real-time monitoring based on the RS-485 communication protocol. A vacuum pump (KNF Nueberger Inc., Model N816.3KN. 18) and a pressure controller (MKS Instruments Inc., Type 640) were used to pump outside gas and control the pressure to be ~40 Torr for narrowing the absorption line. Furthermore, a compact power supply module with a direct current supply voltage of 24 V was developed for the sensor with a total power dissipation of ~36W.

For the sensor operation in the deep-sea environment, a barrel-shape structure with a volume of Φ24.5 × 50 cm was designed for the integration of the sensor, as described by the computer-aided design (CAD) image in Fig. 3(b). Figure 3(c) shows the photograph of the integrated CO_2 sensor system without the barrel-shape cover. The optical sub-system was mounted on the upper side of the baseplate and the electrical sub-system was fixed on the other side to save space.

Optics EXPRESS

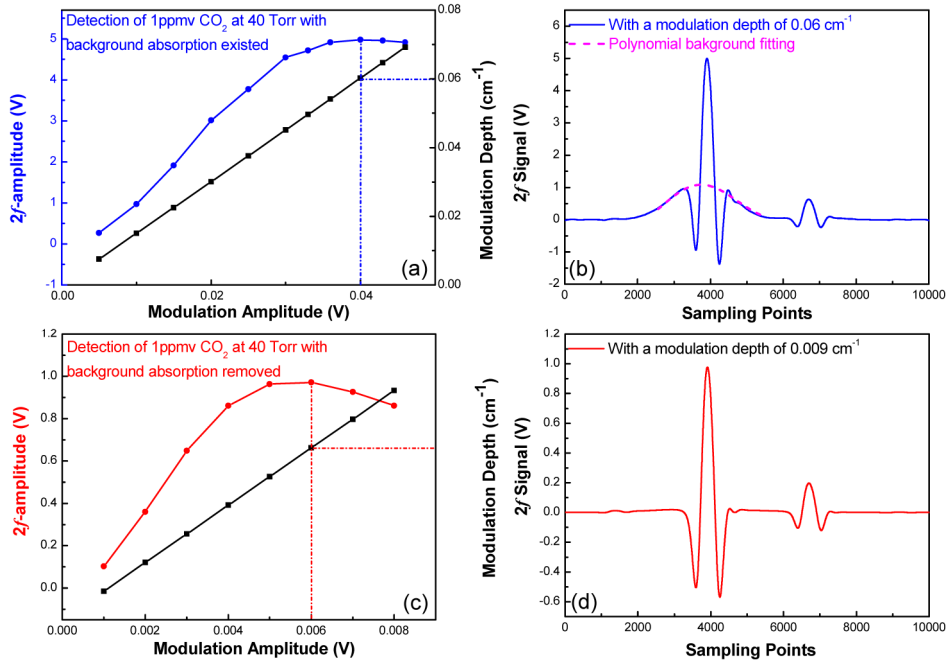

Fig. 4. (a) Modulation depth optimization performed at a CO_2 concentration level of 1 ppmv considering the background absorption. (b) The distorted 2*f* waveform with a modulation depth of 0.06 cm^{-1} and a polynomial background fitting. (c) Modulation depth optimization performed with the background absorption removed. (d) The non-distorted 2*f* waveform obtained with an optimized modulation depth of 0.009 cm^{-1}.

2.4 Modulation depth optimization

Basically, a high 2*f* signal amplitude requires that the modulation depth should be 1.1 times of the full width at half maximum (FWHM) of the selected absorption line. In the developed CO_2 sensor, the FWHM of the target absorption line (0.0093 cm^{-1}) is far less than that of the background absorption (0.1516 cm^{-1}) because of the ultra-low pressure of 40 Torr in the MPGC. To increase the signal-noise ratio (SNR) of the 2*f* signal, optimization of modulation depth was performed using a standard gas sample of 1 ppmv at a pressure of 40 Torr, as plotted in Fig. 4(a). The maximum 2*f*-amplitude was achieved at the modulation depth of 0.06 cm^{-1}, which was already ~6 times of the FWHM of the target absorption line because of the contribution of the background absorption as expressed by the blue line in Fig. 4(b). A polynomial fitting was further performed to deduct the background absorption represented by the pink dash line in Fig. 4(b). As Fig. 4(c) depicts, another modulation depth optimization was carried out with the background absorption removed. When the modulation depth is up to 0.009 cm^{-1} that is nearly equal to the FWHM of the target absorption line, the 2*f*-amplitude reaches the maximum value. The 2*f* signal of one scanning period at the optimum modulation depth of 0.009 cm^{-1} was recorded and the results are shown in Fig. 4(d), where the background absorption is observably suppressed. Consequently, the modulation depth was decided to be 0.009 cm^{-1} with a modulation amplitude of 0.006 V.

Optics EXPRESS

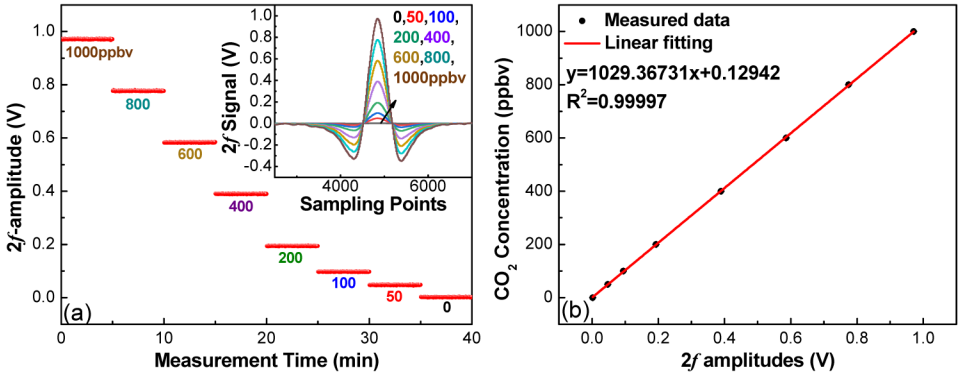

Fig. 5. (a) The recorded 2*f* signal and curves of the 2*f*-amplitude for eight different CO_2 concentration levels of 1000, 800, 600, 400, 200, 100, 50 and 0 ppbv. (b) Measured data dots and linear fitting curve of the CO_2 concentration versus 2*f* signal amplitude.

3. Laboratory measurement of CO_2 sensor system

3.1 Calibration of CO_2 sensor using 2315.19 cm^{-1} line

To target the CO_2 absorption line at 2315.19 cm^{-1}, the ICL temperature and the pressure in the gas cell were set to 0 °C and 40 Torr, respectively. A scan signal with a frequency of 0.5 Hz was generated from the lock-in module and added to the laser current driver to produce a scan current at a range of 47–51 mA, which enabled the ICL to emit at a wavenumber within 2315.05–2315.4 cm^{-1}. A sinusoidal signal with an amplitude of 0.006V and a frequency of 15 kHz was also added to the driving signal to modulate the ICL. The demodulated 2*f* signal was acquired by the DAQ module with a sampling rate of 10 kHz, resulting in a 2×10^4 data points per scanning period. The last 0.9×10^4 points were sampled to target the 2*f* signal of the 2315.19 cm^{-1} line. A gas mixing system (Series 4000, Environics, USA) was used to generate a series of CO_2 samples by diluting a standard 5 ppmv CO_2 with pure nitrogen (N_2) to calibrate the sensor. At each concentration level, an example of the acquired 2*f* waveform was recorded and the measured 2*f* signal amplitude was continuously recorded for 5 minutes, as shown in Fig. 5(a). Then, the 2*f*-amplitude of each concentration were averaged and plotted as a function of the actual concentration value. As depicted in Fig. 5(b), via a linear data-fitting, an equation between the 2*f*-amplitude (max(2*f*)) and the CO_2 concentration (*C*) is obtained as

$$C = 1029.36731 \max(2f) + 0.12942 \quad (2)$$

which can be used to determine the CO_2 concentration according to the measured 2*f*-amplitude.

3.2 Calibration of CO_2 sensor using 2315.28 cm^{-1} line

Due to a strong absorption of $^{12}CO_2$ at 2315.19 cm^{-1}, a saturation phenomenon will occur when the concentration is higher than ~6 ppmv. What's more, the 2*f* signal generated from the absorption of $^{13}CO_2$ appears when the CO_2 concentration exceeds ~20 ppmv. Figure 6(a) exhibits the sampled 2*f* signal of one scanning period at a concentration level of 20 ppmv, indicating the potential of the sensor to simultaneously detect CO_2 concentration and isotope abundance of $^{13}CO_2/^{12}CO_2$. An additional calibration was performed using the weaker $^{12}CO_2$ absorption line of 2315.28 cm^{-1} to achieve a wide detection range of CO_2 concentration. Five CO_2 samples with a concentration range of 0–40 ppmv were prepared by the gas mixing system via diluting a standard 50 ppmv CO_2 with N_2. Similar to the operation in Section 3.1, the measured 2*f*-amplitude of each concentration were averaged and plotted in Fig. 6(b). A

Optics EXPRESS

good linear relation between the averaged 2*f*-amplitude (max(2*f*)) and CO_2 (*C*) concentration level is observed and expressed as

$$C = 5.07786 \max(2f) + 0.01141 \quad (3)$$

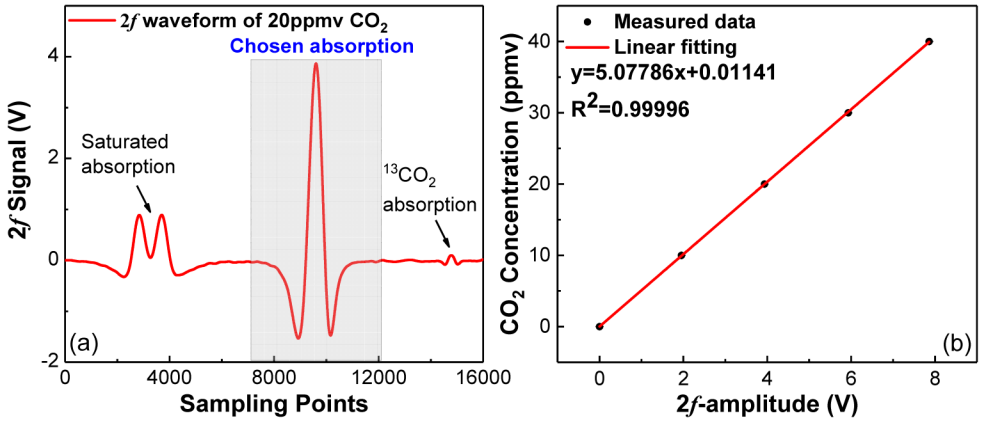

Fig. 6. (a) Recorded 2*f* signal of one scan period at the CO_2 concentration level of 20 ppmv. (b) Experimental measured data and linear fitting curve of CO_2 concentration versus max(2*f*) based on the 2315.28 cm^{-1} absorption line.

3.3 Stability

With a data sampling period of ~2 s, the 2*f* signal amplitude under pure N_2 atmosphere was sampled and recorded for ~30 minutes to evaluate the noise level of the sensor. Using Eq. (2), CO_2 concentration levels were obtained from the measured 2*f*-amplitude and plotted in Fig. 7(a). The fluctuation range of the concentration value was −2–2 ppbv during the whole measurement procedure. An Allan deviation analysis was implemented on the data to characterize the stability, as plotted on a log-log scale versus the averaging time in Fig. 7(b). A limit of detection (LoD) of 0.72 ppbv for a 2 s averaging time and a minimum LoD of 38.9 parts per trillion by volume (pptv) for an optimum averaging time of 124 s were obtained based on the analysis. The theoretical performance of a system impacted only by White-Gaussian noise is expressed by the red line proportional to 1/sqrt(*τ*). A LoD of 0.72 ppbv results in a CO_2 absorbance of 1.7×10^{-4}, which indicates that the CO_2 sensor system effectively restrains the disturbance from the background absorption and achieved a good performance after optimization.

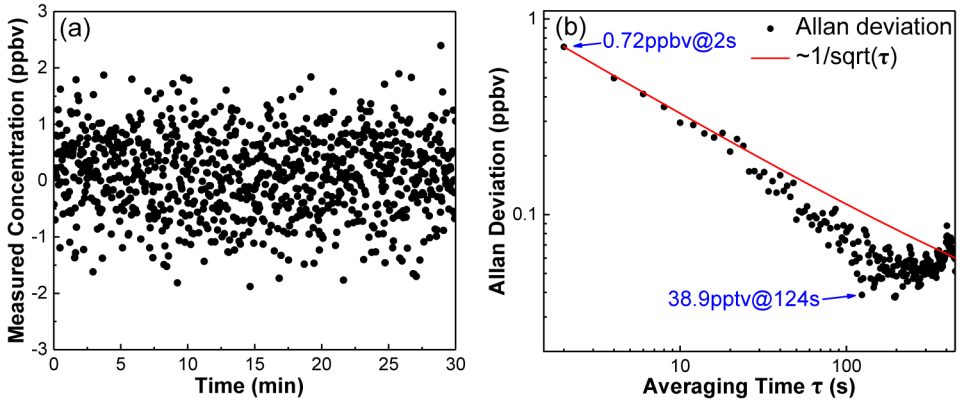

Fig. 7. (a) Long-term concentration measurement of CO_2 by passing pure N_2 into the gas cell. (b) Allan deviation analysis of the sensor based on the data shown in Fig. 7(a).

Optics EXPRESS

3.4 Response time

A dual-stream gas flow path was established (Fig. 8(a)) to assess the response characteristics of the sensor. Pure N_2 and a 1 ppmv CO_2 generated from the gas mixing system were switched by two needle valves to be injected into the gas cell, respectively. Three exchanges were performed between the two gas streams to observe the response, and the measured results were recorded for ~3 min at each concentration level after each exchange, as plotted in Fig. 8(b). A flow controller was employed to indicate the gas flow rate, which was determined to be 180 standard cubic centimeters per minute (sccm). The rise time and fall time are both found to be ~30 s. Overshoots of the measured concentration levels occur at the rise edge because of an instantaneous increscent of the pressure in the MPGC.

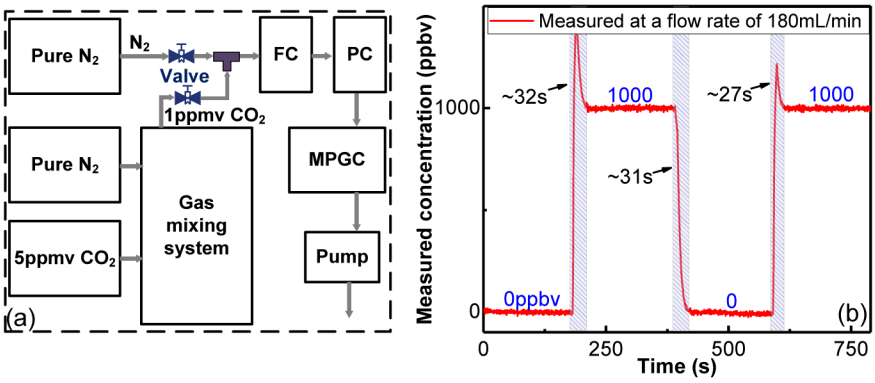

Fig. 8. (a) Schematic diagram of the dual-stream gas flow path for the response time assessment of the sensor. (b) Response time measurements by switching the two gas samples repeatedly.

4. Deployment of CO_2 sensor system with gas-liquid separator

Assisted by a gas-liquid separator system, the developed CO_2 sensor was deployed for the measurement of the dissolved CO_2 in water. Figure 9(a) is a schematic diagram of the deployment of the whole system. Due to a limitation of the gas extraction efficiency, the gas-liquid separator could only generate a gas flow rate of ~2.5 sccm, which was far less than the required 180 sccm for generating a gas pressure of 40 Torr in the MPGC. Therefore a pure N_2 was used as a carrier gas to stabilize the pressure and two flow controllers were employed to limit the flow rate of N_2 and the extracted gas at 177.5 sccm and 2.5 sccm, respectively. The extracted gas carried by N_2 with a dilution ratio of 2.5:180 passed into the CO_2 sensor for detection. Figure 9(b) is a photograph of the sensor connected with the gas-liquid separator.

Optics EXPRESS

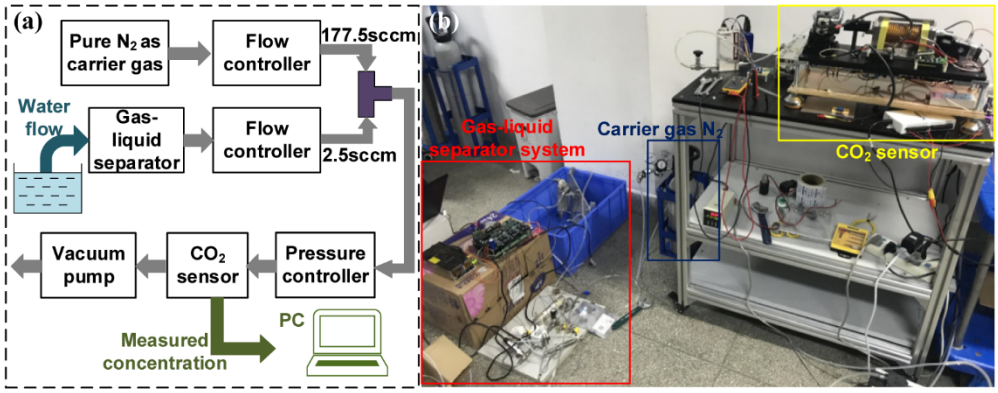

Fig. 9. (a) Schematic diagram and (b) photograph of the sensor system for the deployment in the detection of the dissolved CO_2 in water assisted by a gas-liquid separator and carrier gas.

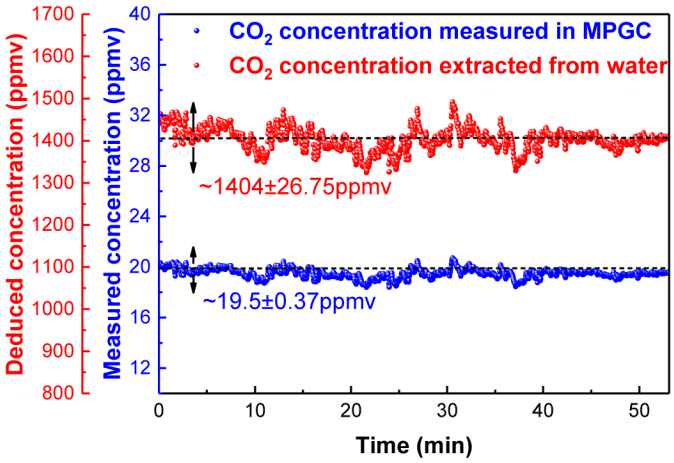

Fig. 10. Measured concentration levels of CO_2 in the gas cell (represented by blue plots) and correspondingly deduced concentration levels of CO_2 extracted from water (represented by red plots) during the deployment of the sensor combined with a gas-liquid separator.

By targeting the weak absorption line, measurements of the gas extracted from water were performed for ~1 hour. The measured concentration values in the MPGC and the deduced values according to the dilution ratio are plotted versus measurement time, as shown in Fig. 10. According to the measurement results, the CO_2 concentration of the gas extracted by the gas-liquid separator is determined to be ~1404 ± 26.75 (1σ) ppmv with a relatively high fluctuation caused by the instability of the flow rate of the extracted gas and carrier gas. For a highly precise detection, a gas-liquid separator with higher efficiency and a flow controller with a better performance are expected in the future.

5. Conclusions

Aiming at deep-sea natural gas hydrate exploration, we reported, for the first time to our knowledge, the development of an ICL-based mid-infrared CO_2 sensor system. A compact rectilinear optical structure as well as a TLAS technique was employed in gas detection. The optical sub-system and electrical sub-system were assembled into a standalone barrel-shape system for minimized size and pressure resistance in deep-sea environment. The ICL was operated to target a strong CO_2 absorption line located at 2315.19 cm^{-1} and a weak 2315.28 cm^{-1} line at a low pressure of 40 Torr. Sensor calibration within a concentration range of 0-1000 ppbv and 0-40 ppmv was performed and a series of experiments were carried out to

Optics EXPRESS

assess the stability and response performances of the sensor. Based on an Allan deviation analysis, a LoD of ~0.72 ppbv at a 2 s averaging time was obtained and at an optimum averaging time of 124 s, the LoD was reduced to ~38.9 pptv. The response time at a dynamic operation was measured to be ~30 s at a gas flow rate of 180 sccm. A field deployment of the sensor together with a gas-liquid separator was reported for the detection of the dissolved CO_2 in water, which validated the normal operation of the sensor system for deep-sea natural gas hydrate exploration.

Funding

The National Key R&D Program of China (2016YFC0303902), National Natural Science Foundation of China (61775079, 61627823), Science and Technology Development Program of Jilin Province, China (20180201046GX, 20190101016JH), Industrial Innovation Program of Jilin Province, China (2017C027), and the National Science Foundation (NSF) ERC MIRTHE award and Robert Welch Foundation (C0586).

Acknowledgments

The authors wish to express their thanks to Dr. Zhen Xu for his assistance with the design and fabrication of the mechanical enclosure, China University of Geosciences for providing the gas-liquid separator system, and Prof. Xiaoming Gao for providing the deployment laboratory.

References

1. B. U. Haq, "Natural gas deposits: methane in the deep blue sea," Science **285**(5427), 543–544 (1999).
2. M. Parlaktuna and T. Erdogmus, "Natural gas hydrate potential of the black sea," Energy Sources **23**, 203–211 (2010).
3. J. Swinnerton, V. Linnenbom, and C. Cheek, "Determination of dissolved gases in aqueous solutions by gas chromatography," Anal. Chem. **34**(4), 483–485 (1962).
4. J. W. Swinnerton and V. J. Linnenbom, "Gaseous hydrocarbons in sea water: determination," Science **156**(3778), 1119–1120 (1967).
5. L. P. Atkinson and F. A. Richards, "The occurence and distribution of methane in the marine environment," Deep-Sea Res. Oceanogr. Abstr. **14**(6), 673–684 (1967).
6. W. J. Lv, I. M. Chou, and R. C. Burruss, "Determination of methane concentrations in water in equilibrium with sI methane hydrate in the absence of a vapor phase in situ Raman spectroscopy," Geochim. Cosmochim. Acta **72**(2), 412–422 (2007).
7. S. Ker, Y. Le Gonidec, B. Marsset, G. K. Westbrook, D. Gibert, and T. A. Minshull, "Fine-scale gas distribution in marine sediments assessed from deep-towed seismic data," Geophys. J. Int. **196**(3), 1466–1470 (2014).
8. D. G. Lancaster, R. Weidner, D. Richter, F. K. Tittel, and J. Limpert, "Compact CH_4 sensor based on difference frequency mixing of diode lasers in quasi-phasematched $LiNbO_3$.," Opt. Commun. **175**(4-6), 461–468 (2000).
9. D. G. Lancaster and J. M. Dawes, "Methane detection with a narrow-band source at 34 μm based on a Nd:YAG pump laser and a combination of stimulated Raman scattering and difference frequency mixing," Appl. Opt. **35**(21), 4041–4045 (1996).
10. C. Fischer and M. W. Sigrist, "Trace-gas sensing in the 3.3-μm region using a diode-based difference-frequency laser photoacoustic system," Appl. Phys. B **75**(2–3), 305–310 (2002).
11. D. Richter, D. G. Lancaster, R. F. Curl, W. Neu, and F. K. Tittel, "Compact mid-infrared trace gas sensor based on difference-frequency generation of two diode lasers in periodically poled $LiNbO_3$," Appl. Phys. B **67**(3), 347–350 (1998).
12. K. P. Petrov, S. Waltman, E. J. Dlugokencky, M. Arbore, M. M. Fejer, F. K. Tittel, and L. W. Hollberg, "Precise measurement of methane in air using diode-pumped 3.4-μm difference-frequency generation in PPLN," Appl. Phys. B **64**(5), 567–572 (1997).
13. J. A. Silver, "Frequency-modulation spectroscopy for trace species detection: theory and comparison among experimental methods," Appl. Opt. **31**(6), 707–717 (1992).
14. P. Werle, "A review of recent advances in semiconductor laser based gas monitors," Spectrochim. Acta A **54**(2), 197–236 (1998).
15. S. Schilt, L. Thévenaz, and P. Robert, "Wavelength modulation spectroscopy: combined frequency and intensity laser modulation," Appl. Opt. **42**(33), 6728–6738 (2003).
16. G. Wysocki, Y. Bakhirkin, S. So, F. K. Tittel, C. J. Hill, R. Q. Yang, and M. P. Fraser, "Dual interband cascade laser based trace-gas sensor for environmental monitoring," Appl. Opt. **46**(33), 8202–8210 (2007).
17. M. N. Fiddler, I. Begashaw, M. A. Mickens, M. S. Collingwood, Z. Assefa, and S. Bililign, "Laser spectroscopy for atmospheric and environmental sensing," Sensors (Basel) **9**(12), 10447–10512 (2009).

Optics EXPRESS

18. R. F. Curl, F. Capasso, C. Gmachl, A. A. Kosterev, B. McManus, R. Lewicki, M. Pusharsky, G. Wysocki, and F. K. Tittel, "Quantum cascade lasers in chemical physics," Chem. Phys. Lett. Front. Artic. **487**(1-3), 1–18 (2010).
19. G. Wysocki, A. A. Kosterev, and F. K. Tittel, "Spectroscopic trace-gas sensor with rapidly scanned wavelengths of a pulsed quantum cascade laser for in situ NO monitoring of industrial exhaust systems," Appl. Phys. B **80**(4-5), 617–625 (2005).
20. M. Lewander, Z. G. Guan, L. Persson, A. Olsson, and S. Svanberg, "Food monitoring based on diode laser gas spectroscopy," Appl. Phys. B **93**(2-3), 619–625 (2008).
21. R. Q. Yang, J. D. Bruno, J. L. Bradshaw, J. T. Pham, and D. E. Wortman, "High power interband cascade lasers with quantum efficiency >450%," Electron. Lett. **35**(15), 1254–1255 (1999).
22. R. Q. Yang, "Mid-infrared interband cascade lasers based on type-II heterostructures," Microelectronics J. **30**(10), 1043–1056 (1999).
23. J. L. Bradshaw, R. Q. Yang, J. D. Bruno, J. T. Pham, and D. E. Wortman, "High-efficiency interband cascade lasers with peak power exceeding 4W/facet," Appl. Phys. Lett. **75**(16), 2362–2364 (1999).
24. J. H. Miller, Y. A. Bakhirkin, T. Ajtai, F. K. Tittel, C. J. Hill, and R. Q. Yang, "Detection of formaldehyde using off-axis integrated cavity output spectroscopy with an interband cascade laser," Appl. Phys. B **85**(2–3), 391–396 (2006).
25. C. T. Zheng, W. L. Ye, N. P. Sanchez, C. G. Li, L. Dong, Y. D. Wang, R. J. Griffin, and F. K. Tittel, "Development and field deployment of a mid-infrared methane sensor without pressure control using interband cascade laser absorption spectroscopy," Sens. Actuators B Chem. **244**, 365–372 (2017).
26. W. Ye, C. Li, C. Zheng, N. P. Sanchez, A. K. Gluszek, A. J. Hudzikowski, L. Dong, R. J. Griffin, and F. K. Tittel, "Mid-infrared dual-gas sensor for simultaneous detection of methane and ethane using a single continuous-wave interband cascade laser," Opt. Express **24**(15), 16973–16985 (2016).
27. Z. W. Liu, C. T. Zheng, C. Chen, H. T. Xie, Q. Ren, W. L. Ye, Y. D. Wang, and F. K. Tittel, "A near-infrared carbon dioxide sensor system using a compact folded optical structure for deep-sea natural gas hydrate exploration," Anal. Methods **10**(39), 4838–4844 (2018).
28. D. B. Oh, M. E. Paige, and D. S. Bomse, "Frequency modulation multiplexing for simultaneous detection of multiple gases by use of wavelength modulation spectroscopy with diode lasers," Appl. Opt. **37**(12), 2499–2501 (1998).
29. H. X. Cui, Z. H. Du, W. L. Chen, R. B. Qi, and K. X. Xu, "Applying diode laser wavelength modulation spectroscopy to detect oxygen concentration," Lasers Eng. **18**, 263–270 (2008).